Nonuniformity Correction Algorithm Based on a Noise-Cancellation System for Infrared Focal-Plane Arrays *

Sebastián E. Godoy[a], Sergio N. Torres[a], Jorge E. Pezoa[b], Majeed M. Hayat[b] and Qi Wang[c]

[a] Department of Electrical Engineering,
Universidad de Concepción, Casilla 160-C, Concepción, Chile;

[b] Department of Electrical and Computer Engineering,
The University of New Mexico, Albuquerque, NM 87131-1356, USA;

[c] Department of Electrical and Computer Engineering,
Shanghai Jiao Tong University, Shanghai, China.

ABSTRACT

In this paper a novel nonuniformity correction method that compensates for the fixed-pattern noise (FPN) in infrared focal-plane array (IRFPA) sensors is developed. The proposed NUC method compensates for the additive component of the FPN statistically processing the read-out signal using a noise-cancellation system. The main assumption of the method is that a source of noise correlated to the additive noise of the IRFPA is available to the system. Under this assumption, a finite impulse response (FIR) filter is designed to synthesize an estimate of the additive noise. Moreover, exploiting the fact that the assumed source of noise is constant in time, we derive a simple expression to calculate the estimate of the additive noise. Finally, the estimate is subtracted to the raw IR imagery to obtain the corrected version of the images. The performance of the proposed system and its ability to compensate for the FPN are tested with infrared images corrupted by both real and simulated nonuniformity.

Keywords: Focal-Plane Arrays, Nonuniformity Correction, Noise-Cancellation System, Additive Noise, Fixed-Pattern Noise.

1. INTRODUCTION

The nonuniformity is an undesirable problem present in infrared (IR) focal-plane arrays (FPA), which manifest itself as a different response at each detector, even though they receive the same input irradiance and they were fabricated with the same material and technique. Therefore, an IRFPA system can show significant differences in its responsivity, gain and noise, which produces the usually called **Spatial Noise**. Other deterioration factor that is inherent to the detectors, is the electronic or thermal noise which is commonly called **Temporal Noise** and it is produced in the semiconductor devices due to the random flow of carriers and the interaction among them. With this background, the problem could be divided in two components: (i) an additive temporal noise which varies frame to frame, and (ii) an almost-time-invariant, compared with the additive temporal noise, additive and multiplicative spatial-noise usually called Fixed-Pattern Noise (FPN).[1–3] In the literature, the additive and multiplicative components of the FPN are also called the gain and the bias NU, respectively.

* This work was partially supported by Grants Milenio ICM P02-049 and by FONDECYT 1060894 and 7060120. The authors wish to thank Ernest E. Armstrong (OptiMetrics Inc., USA) for collecting the data, and the United States Air Force Research Laboratory, Ohio, USA.

Further author information: (Send Information to S.E.G.)
S.E.G. and S.N.T.: E-mail: segodoy@udec.cl, sertorre@udec.cl, FAX: (56) 41 224-6999; TEL: (56) 41 220-3005;
J.E.P. and M.M.H.: E-mail: jpezoa@ece.unm.edu, hayat@ece.unm.edu, FAX (505) 277-1439; TEL (505) 277-0297;
Q.W.: E-mail:jackickwelch@gmail.com

Several techniques has been developed to perform the nonuniformity correction (NUC), nevertheless the problem is still challenging without a complete solution. One of the most basic and effective solution is the radiometric calibration of the camera.[4,5] Radiometric calibration is achieved by using one or more black-body radiators or similar sources of temperature, but in some cases it is not useful enough because it involves the interruption of the camera's operation. To avoid such disadvantages, signal-processing techniques has been also developed. These methods rely on both the diversity in the irradiance integrated by the IRFPA and the motion of the scene that is being imaged.[6–8]

This paper proposes a new signal-processing technique based on the well-known noise-cancellation (NC) technique, which is used to recover signals corrupted by additive noise as in the case of loudspeaker telephone systems in cars and echo path cancellation in telephone networks among others applications.[9] Our proposed NC-based NUC method relies on the main assumption that the additive component of the FPN in an IRFPA is correlated to some additional source of noise available to use. Thus, given this additional source of noise, we synthesize a replica of the bias NU by means of an finite impulse response (FIR) filter, whose coefficients are designed in order to minimize the mean-square error (MSE) between the bias NU and the supplementary source of noise. In addition, given that the supplementary source of noise is constant in time, we take advantage of this situation to obtain an explicit formula to calculate the estimate of the bias NU. Such estimate is then subtracted from the raw IR imagery to obtain sets of images compensated for the additive component of the FPN.

2. NOISE SOURCES ON AN IR-FPA

As in any sensors and arrays, the IRFPA performance assessment requires the identification and quantitative representation of its noise sources, especially when the elimination of these sources is desired.

Every single detector has some known sources of noise like johnson, shot and flicker noise, but for a complete FPA system, there are some additional sources that also must be consider, and mainly there are given by FPA temporal noise, FPA spatial noise, and the readout noise given by the output electronics.[1,2]

The **temporal noise** varies frame-to-frame, whereas FPN does not, and depending of the technology used in the fabrication of the detectors and the readout structure, it could varies pixel-to-pixel.[2] Temporal readout-noise and dark-level noise are not function of sensor exposure. However quantum noise depends of the input infrared irradiance.[1] The *quantum noise* is given by a non-ideal photo-detection process and it is determinate by the pixel exposure, the pixel spacing and the quantum noise factor which (for a given exposure) is the ratio of measured quantum-noise variance to shot-noise variance. It represents the excess noise not accounted by Poisson statistics. A factor which gives rise to the departure from the ideal photodetection is the presence of gain in the sensor (more than one carrier is generated for a single photon interaction). The *additive temporal noise* has its origin in the FPA dark current, for its temperature dependence, and in the readout circuitry, including the readout amplifier and poor charge-transfer efficiency (CTE), which is the ability to transfer all the charge from one step to the next.[2]

The **fixed-pattern noise** refers to any spatial pattern that does not change significantly from frame-to-frame, and it is due to differences in detectors size, doping density and foreign matter getting trapped during fabrication. The *multiplicative FPN* is due by the FPA photoresponse nonuniformity, which means that the responsivity (when light is applied) varies from detector to detector. This implies that it is produced by pixel-to-pixel differences in responsivity or gain, the detector size, spectral response and thickness in coatings of each detector. The *additive FPN* is due mainly by the dark current which is kept almost constant and does not vary frame-to-frame by its dependence to the temperature, showing up fluctuations which creates a pattern noise,[2] and by the offset voltages due to the amplifiers used (on-chip and off-chip) which consist in two components: 1/f noise and white-noise.

In Table 1 we list a summary of the principal noise types and its dependence to the incident radiation in the detectors. This gives rise to the mathematical linear model of the FPA which will be discuss in the following section.

Table 1. Principal noise types and its dependence with the incident radiation

	Dependence	**Noise type**
Temporal	Additive	Readout noise (amplifiers and poor charge-transfer efficiency).
	Multiplicative	Quantum noise.
FPN	Additive	Dark-level and some readout patterns.
	Multiplicative	Responsivity.

3. MATHEMATICAL MODEL FOR FPN IN IR-FPA

3.1. Detector's Mathematical Model

In an IR-FPA each detector converts the incident infrared energy at the input into electrical energy like current or voltage information at its output. Unfortunately the input-output characteristics of detectors vary from one detector to another, in spite of the fact that they were fabricated under identical conditions. In addition, the characteristics of the same detector might drift over time because of changes in external conditions, and generally it cannot be modeled accurately in a deterministic fashion.[8]

As was stated in the previous section, the detector's response is usually modeled as a first-order relationship between the input irradiance and its output, which includes gain and bias for each detector resuming the different noises present in the FPA system. Then, for the $(i,j)^{th}$ detector in the FPA, the k-th time-sample can be expressed as:

$$Y_{i,j}[k] \;=\; A_{i,j}[k] \cdot X_{i,j}[k] \;+\; B_{i,j}[k] \;+\; V_{i,j}[k] \tag{1}$$

where $A_{i,j}[k]$ and $B_{i,j}[k]$ are the gain and the bias of the $(i,j)^{th}$ detector, $V_{i,j}[k]$ is the additive temporal noise and $X_{i,j}[k]$ represents the true irradiance. Moreover, according to the Table 1, the relationship between each variable and which really represents can easily addressed. This means that the gain $A_{i,j}[k]$ represents both quantum and responsivity noises, the offset $B_{i,j}[k]$ represents the detectors' dark-level and some readout patterns given by the readout technology, and finally the temporal noise factor $V_{i,j}[k]$ represents the readout problems like poor charge-transfer efficiency and reset noise given by an undesirable number of electrons which stay in the capacitor after the lecture.

As in several approaches, we will introduce some simplifications to the aforementioned model. Firstly, the temporal noise will not be considered in the formulation of our algorithm. In addition, given that the algorithm will be developed over a block of frames representing no more than a few minutes, the gain and bias variations within the block in each pixel will be also consider negligible, thus $A_{i,j}[k] \approx A_{i,j}$ and $B_{i,j}[k] \approx B_{i,j}$.[8,10] We will synthesize the additive component of the FPN, so let us define $S_{i,j}[k] = A_{i,j} \cdot X_{i,j}[k]$, which indirectly involves the assumption that the gain is constant and equal to unity among all detectors and it is due to the observation that in many operational conditions, the bias-nonuniformity typically dominates gain-nonuniformity.[8,11,12] Under these simplifying assumptions, the Equation (1) reduces to

$$Y_{i,j}[k] \;=\; S_{i,j}[k] \;+\; B_{i,j}\ , \tag{2}$$

which will be used in the development of our algorithm. Finally, to simplify the notation, from now on the pixel superscripts i,j are dropped out with the understanding that all operations are performed on a pixel-by-pixel basis.

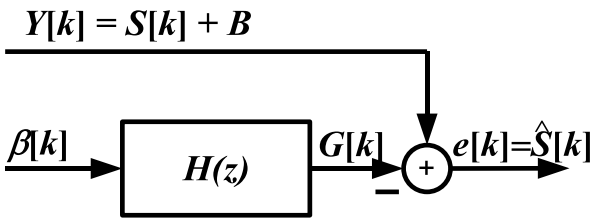

Figure 1. Block diagram of the Noise-Cancellation–Based algorithm.

4. THE NOISE-CANCELLATION–BASED NUC ALGORITHM

Let us consider the block-diagram shown in Figure 1, where the input signal $Y[k]$ is the superposition of the additive component of the FPN, B, and the product between the gain and the true irradiance, $S[k]$. Assume that the signal $\beta[k]$ is statistically correlated to B, i.e., assume that a source of noise statistically correlated to the additive component of the FPN is available to the system. If the filter's output, $G[k]$, is a fairly good approximation of B, then the output error will be a good estimation of the true irradiance, $e[k] = \hat{S}[k]$. Therefore, we can estimate the additive component of the FPN by properly designing the filter, and thus obtaining an estimation of the true irradiance $S[k]$ at the system's output. Clearly, the analysis relies on the assumption that B can be estimated from $\beta[k]$. This assumption is not restrictive, but it imposes the requirement that $\beta[k]$ must be a signal with the same statistics as B, consequently, the performance of the NC system strongly depends on the correlation between them. According to the previous assumption that the bias is constant among the time-window considered, the correlated noise should be assumed constant too, thus $\beta[k] \approx \beta$.

4.1. Least-Squares Design of the Bias Compensator

Let us consider now that the NC system synthesize $G[k]$ using a LTI FIR filter with N coefficients denoted by $h_k,\ k = 0, \ldots, N-1$. Assume also that for the time-window considered, $Y[k]$ and β are stationary random processes. Thus, according to least squares theory we calculate the MSE of the estimate of B as:

$$MSE = \mathsf{E}\left[e[k]^2\right] = \phi_{YY}[0] - 2\sum_{i=0}^{N-1} h_i \phi_{\beta Y}[i] + \sum_{i=0}^{N-1}\sum_{j=0}^{N-1} h_i h_j \phi_{\beta\beta}[i-j] \tag{3}$$

where $\phi_{YY}[n]$ and $\phi_{\beta\beta}[n]$ are the autocorrelation sequences of $Y[k]$ and β, respectively, and $\phi_{\beta Y}[n]$ is the cross-correlation sequence between β and $Y[k]$.

During the design process, we are looking for the vector of optimal filter coefficients, $\mathbf{h}_N^*$, that minimize the error between $G[k]$ and B in the mean square sense. So, after taking first order partial derivatives of the Equation (3) with respect to every h_k and setting them equal to zero, we obtain a system of N linear equations for the filter coefficients. The system of equations as well as its solution can be written in matrix form as:

$$\mathbf{\Phi}_{\beta\beta} \cdot \mathbf{h}_N = \mathbf{\Phi}_{\beta Y} \tag{4}$$

$$\mathbf{h}_N^* = \mathbf{\Phi}_{\beta\beta}^{-1} \cdot \mathbf{\Phi}_{\beta Y}, \tag{5}$$

where:

$$\begin{aligned}
\mathbf{\Phi}_{\beta\beta} &= \begin{bmatrix} \phi_{\beta\beta}[0] & \phi_{\beta\beta}[1] & \phi_{\beta\beta}[2] & \cdots & \phi_{\beta\beta}[N-1] \\ \phi_{\beta\beta}[1] & \phi_{\beta\beta}[0] & \phi_{\beta\beta}[1] & \cdots & \phi_{\beta\beta}[N-2] \\ \phi_{\beta\beta}[2] & \phi_{\beta\beta}[1] & \phi_{\beta\beta}[0] & \cdots & \phi_{\beta\beta}[N-3] \\ \vdots & \vdots & \vdots & \ddots & \vdots \\ \phi_{\beta\beta}[N-1] & \phi_{\beta\beta}[N-2] & \phi_{\beta\beta}[N-3] & \cdots & \phi_{\beta\beta}[0] \end{bmatrix} \\
\mathbf{h}_N &= \begin{bmatrix} h_0 & h_1 & h_2 & \ldots & h_{N-1} \end{bmatrix}^T \\
\mathbf{\Phi}_{\beta Y} &= \begin{bmatrix} \phi_{\beta Y}[0] & \phi_{\beta Y}[1] & \phi_{\beta Y}[2] & \ldots & \phi_{\beta Y}[N_B-1] \end{bmatrix}^T .
\end{aligned}$$

In most of the NC based systems, the signal corresponding to the source of noise correlated to the additive noise corrupting the SoI is obtained directly from the process. In our case, a situation like that implies the use of an uniform source that images the array, i.e., a black-body radiator. The novel approach introduced in our NC based method is that we simulate a black-body radiator source creating a block of spatially flat and temporally constant block images of length K frames. So, using the assumption on the stationarity of the random processes modeling each noise component, we corrupt a block of spatially flat and constant in time images adding a random constant that is assumed to be the source of correlated noise.

Given that β is a random constant during the time-window considered, we can exploit this fact in order to obtain an explicit expression for the sequence of filtered images. Assume that the random process β takes the particular value $\beta_0,\ \beta_0 \neq 0$, for any pixel in the array during the time interval corresponding to K frames. Using the definition of the auto- and cross-correlation sequences, it is straightforward to derive that $\phi_{\beta\beta}[k]$ and $\phi_{\beta Y}[k]$, at the kth lag, are given by

$$\phi_{\beta\beta}[k] = \frac{\beta_0^2(K-k)}{K} \quad , \quad \phi_{\beta Y}[k] = \frac{\beta_0 \sum_{i=0}^{K-1-k} Y[i]}{K} = \frac{\beta_0(K-k)\bar{Y}_{K-k}}{K} \ , \tag{6}$$

where $\bar{Y}_{K-k}$ stands for the temporal average taken from the sample number $i=0$ upto the sample $K-1-k$. Therefore, the solution of the system of linear equations (5) can be written as $\mathbf{h}^* = \frac{1}{\beta_0}\mathbf{\Lambda}_N^{-1} \cdot \mathbf{v}_N$, where the matrix $\mathbf{\Lambda}_N$ and the vector $\mathbf{v}_N$ are given by

$$\begin{aligned}
\mathbf{\Lambda}_N &= \begin{bmatrix} K & K-1 & K-2 & \cdots & K-(N-1) \\ K-1 & K & K-1 & \cdots & K-(N-2) \\ K-2 & K-1 & K & \cdots & K-(N-3) \\ \vdots & \vdots & \vdots & \ddots & \vdots \\ K-(N-1) & K-(N-2) & K-(N-3) & \cdots & K \end{bmatrix} , \\
\mathbf{v}_N &= \begin{bmatrix} K\bar{Y}_K \\ (K-1)\bar{Y}_{K-1} \\ (K-2)\bar{Y}_{K-2} \\ \cdots \\ (K-(N-1))\,\bar{Y}_{K-(N-1)} \end{bmatrix} .
\end{aligned}$$

Furthermore, using matrix notation we can write the output of the NC system as

$$\hat{S}[k] = Y[k] - (\mathbf{h}^*)^T \begin{bmatrix} \beta[k] \\ \beta[k-1] \\ \vdots \\ \beta[k-(N-1)] \end{bmatrix} = Y[k] - \mathbf{v}_N^T \mathbf{\Lambda}_N^{-1} \mathbf{1}_N \ , \tag{7}$$

where the superscript T stands for vector and matrix transposition and the vector $\mathbf{1}_N$ is an all-ones column vector of dimension N. Note that the sequence of compensated images does not depend on the value of β_0, and moreover, for fixed K and N $\mathbf{v}_N^T \mathbf{\Lambda}_N^{-1} \mathbf{1}_N$ is a constant number. A tedius but straightforward calculation, which starts with the matrix $\mathbf{\Lambda}$ and uses the blockwise matrix inversion, lead us to the final expression that is used to compensate for the bias nonuniformity at every pixel of the IR-FPA

$$\hat{S}[k] \quad = \quad Y[k] - \left(\frac{K\bar{Y}_K + (K-(N-1))\,\bar{Y}_{K-(N-1)}}{2K-(N-1)} \right) . \tag{8}$$

Note that for the special case $N = 1$, Equation (8) is $\hat{S}[k] = Y[k] - \bar{Y}_K$. Recalling that $B \approx \bar{Y}_K$, then the proposed NC-based method turns out to be equivalent to the constant statistics algorithm compensating only for the bias nonuniformity.[6,7]

5. PERFORMANCE ANALYSIS OF THE NC-BASED ALGORITHM

There are two parameters that can be accustomed in this method: the number of frames used to calculate the cross-correlation between the read-out data and the source of correlated noise (K), and the number of taps of the FIR filter used to synthesize the additive noise (N). Hence both will be analyzed in attempt to determinate the best algorithm design.

The set of data used in our calculations corresponds to mid-wave IR (3-5 μm) imagery, collected at 1 PM, using a InSb-FPA–based cooled camera (AMBER Model AE-4128). Each image, captured at the rate of 30 fps, has a size of 128×128 pixels and each pixel is quantized in integer values using 16 unsigned bits. In order to study the effect of the block length on the performance of the filters, we varied the parameter K_B from 900 to 1400 frames in increments of 100 blocks. In addition, we also used different number of filter coefficients, $N \in \{1, 2, 3, 4, 5\}$ for every block length considered. The performance metric used is the average, over all pixels and over all frames, MSE between the estimate $\hat{S}[k]$ and the actual irradiance, $X[k]$. In this paper, the actual values of irradiance were obtained compensating for nonuniformity blocks of images using a two-point calibration method. We performed around one hundred trials of Monte-Carlo simulations per experiment, and all the results obtained correspond to the averaged values of the considered metrics over the total number of trials. Our results confirm the accuracy and robustness of the proposed method to estimate the FPN components.

In Fig. 2(a), the results obtained for the evaluation of the number of filter coefficients are depicted. It can be seen that that the average MSE per pixel of the irradiance is almost insensitive to the number of coefficients; this suggests that only one coefficient per filter is enough to attain a good estimation of the noises. Note that the minimum average MSE per pixel is achieved when $K = 1300$, i.e., using a large number frames does not improve the performance of the system. This result is in agreement with the well-known side effect of signal-processing–based nonuniformity correction: ghosting artifacts. Increasing the number of frames improves the nonuniformity correction until some point, after that the new information added to any method produces the effect of imposing artifacts on the compensated images, thereby reducing the performance, which in our case increases the average MSE per pixel. In Fig. 2(b) we show the average MSE per pixel of the irradiance as a function of the block length at the output of the proposed method. In this simulation, we fixed the number of coefficients to $N = 1$. It can be seen that the optimal value effectively is obtained in a time-windows given by $K = 1300$ frames.

6. APPLICATION TO IMAGE SEQUENCES WITH SIMULATED BIAS NONUNIFORMITY

Taking a block of frames previously cleaned with two point calibration and corrupting it with known-bias nonuniformity, the filter is applied in attempt to determinate its capability of remove the additive components

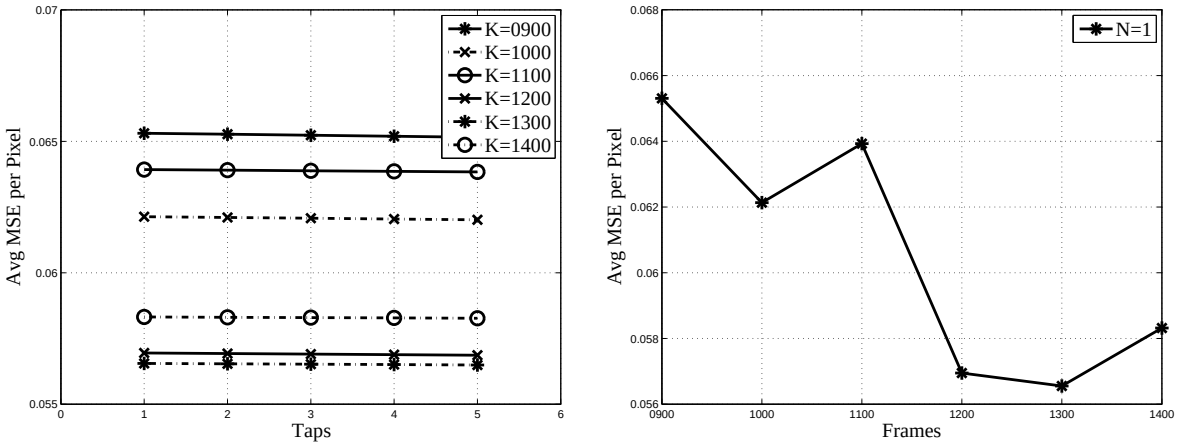

Figure 2. Variations of the Average MSE per pixel by the variation of: (a) Numer of taps of the FIR filter, and (b) Number of frames used to calculate the correlation.

in an artificially corrupted image sequence. The bias is generated as a constant random variable spatially distributed among the normalized camera dynamic range. These parameters are applied over the entire block of previously-cleaned data, which indirectly implies the assumption that the bias nonuniformity is constant amid the block of frames.

The results for different levels of additive noise applied over the AMBER's data are presented, comparing the output image with its raw version and calculating the MSE with respect to the radiometrically corrected imagery. Derived from the previous analysis, the NC-based algorithm was implemented with a one-tap FIR filter and using a block of 1300 frames to calculate the correlation between the different variables. The different values of the metric MSE are also revealed in the Fig. 3 for 10%, 50% and 100% of added noise. These percentages represent the weight of the simulated bias over the normalized dynamic range of the cameras.

To evaluate the performance, the average MSE was used as a metric of the estimation process: The corrupted imagery with 10%, 50% and 100% show an average MSE of 0.3876, 0.4778 and 0.5022 respectably and their corrected versions present an average MSE of 0.0516, 0.0554, and 0.0583. Based in both the naked-eye evaluation of the Fig. 3 and the MSE obtained for each case of corrupted level, the performance of the algorithm eliminating an additive component of noise could be consider successful. Therefore, for this implementation the propose method has shown a very good performance as well as robustness related to the chosen distribution for the additive noise nonuniformity.

7. APPLICATION TO REAL INFRARED IMAGE SEQUENCES

The algorithm was tested using IR data taken with the AMBER camera, where four different block length's were used to calculate the filter coefficients of the gain compensator, namely, $K_A \in \{100, 400, 800, 1300\}$. The filter was implemented with only one tap $N = 1$ according to the previous filter analysis. In Figs. 4(a)-(f) we show a sample image an its corresponding corrected versions obtained in our Monte-Carlo trials. Based on a naked-eye evaluation, the effect of the block length on the image quality of the corrected images is important for little block length's ($K = 100$ and $K = 400$) but it is not distinguishable for high block lengths ($K = 800$ and $K = 1300$); nevertheless, the average MSE effectively is reduced: the average MSE between the two-point

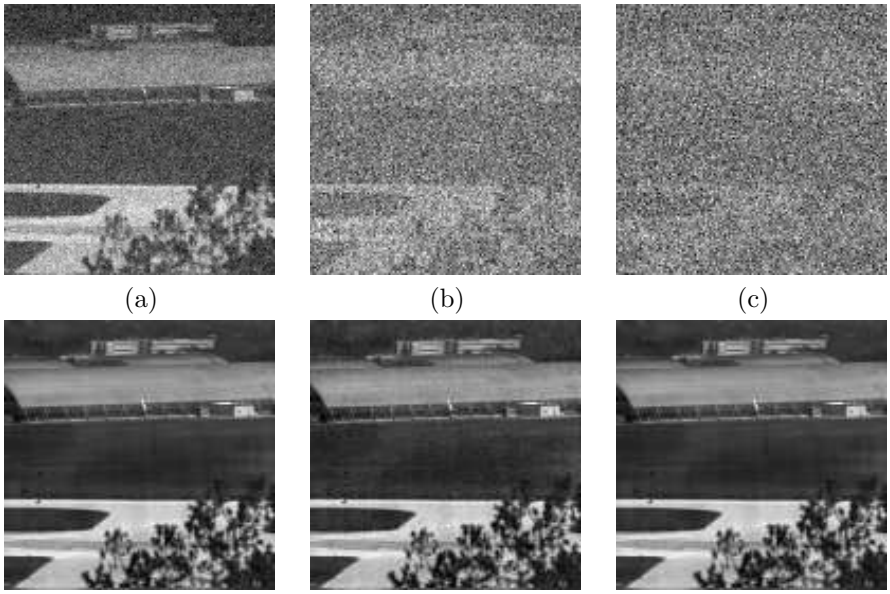

Figure 3. Correction of Simulated Bias Nonuniformity for the AMBER camera corresponding to the $k = 100$th frame. (a) Corrupted Frame with 10%, (b) Corrupted Frame with 50%, (c) Corrupted Frame with 100%, (d) Frame with 10% of simulated bias corrected, (e) Frame with 50% of simulated bias corrected, and (f) Frame with 100% of simulated bias corrected

calibrated image and the compensated images was 0.1363 for $K = 100$, 0.0941 for $K = 400$, 0.0733 for $K = 800$ and 0.0566 for $K = 1300$.

The algorithm was also tested using a second set of real IR data in order to evaluate its performance and the data dependency of the design. The second set of data used corresponds to 7-14μm IR indoor-imagery, collected at 3 PM using an uncooled HgCdTe-FPA–based camera (FLIR Merlin). The frame rate for this set of data is also 30 fps, where the frame size is 320×240 pixels and each pixel is quantized in integers values using 8 unsigned bits. We applied the algorithm on a 128×128 subimage to reduce the total number of mathematical operations but keeping enough information to allow a naked-eye performance evaluation. The sources of correlated noise were specified with the following parameters $\beta \sim U([0, 255])$, and $c_B = 128$. For this set of data, a reference block of images corrected using calibration techniques is not available; therefore, the best block length for this camera was selected based on a naked-eye evaluation of the compensated images. In this experiment, we changed the block lengths K and K_B between 100 and 1500 frames per block in increments of 100 frames to determinate some of the characteristically values of K for the correction. It is interesting to note that according to our subjective evaluation, the best image quality is obtained for a block length of 1300 frames as well as for the AMBER camera.

The results over this set of data are shown in Figs. 5(a)–(e), and as before, the filtered images with block lengths of $K \in \{100, 400, 800, 1300\}$ are depicted. Note that for the FLIR Merlin camera the nonuniformity is much more severe as compared to the nonuniformity present in the AMBER camera. However, at the output of the NC based algorithm, again the nonuniformity level present at the compensated image has decreased significantly, improving the visual quality of the image to an acceptable level.

Finally, in order to obtain a quantitative measurement on the performance of the proposed algorithm we

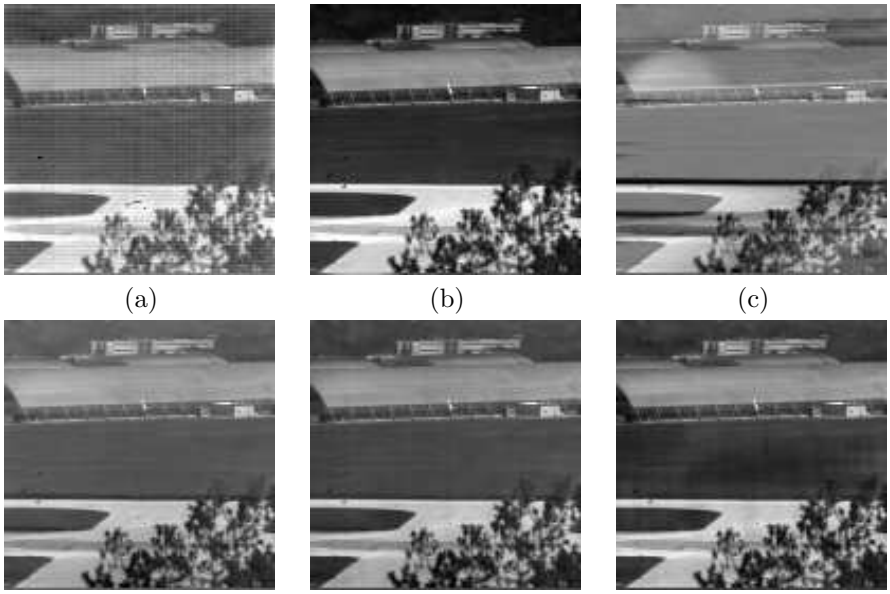

Figure 4. A sample IR image from the block of data of the AMBER camera corresponding to the $k = 100$th frame. (a) The raw image. The compensated versions of the raw image using: (b) the two-point calibration method, (c) the bias compensator algorithm with $K = 100$ frames, (d) the bias compensator algorithm with $K = 400$ frames, (e) the bias compensator algorithm with $K = 800$ frames, and (f) the bias compensator algorithm with $K = 1300$ frames.

employ for the FLIR Merlin IR data the roughness parameter, ρ, which is computed for any image f as:[13]

$$\rho(f) = \frac{\|h_1 * f\|_1 + \|h_2 * f\|_1}{\|f\|_1} \ , \tag{9}$$

where $h_1(i,j) = \delta_{i-1,j} - \delta_{i,j}$, $h_2(i,j) = \delta_{i,j-1} - \delta_{i,j}$, δ_{ij} is the Kronecker delta, $\|f\|_1$ is the ℓ^1-norm of f, and the operator $*$ represents the discrete convolution. Note that ρ is zero for an uniform image and it increases with the pixel-to-pixel variation in the image. Note also that ρ does not require a reference image as in the case of the averaged MSE. Figs. 6(a) and (b) show the computed roughness coefficient of each frame for two different block lengths: $K = 800$ and $K = 1300$ for both cameras. The roughness coefficient was calculated after normalizing each frame to set aside the best comparison. It can be seen that for both sets of data and for the different block lengths the proposed algorithm effectively reduces the roughness coefficient as compared to the raw images.

8. CONCLUSIONS

In this paper, we present a new scene-based NUC technique based on a NC system that compensates for bias nonuniformity in IR imaging systems. The proposed method was reduced to the evaluation of one equation. In light of the results, the assumptions taken regarding the statistical distribution of the FPN components achieved excellent results despite of the uncertainty associated to the actual model of the noise. The strength of the proposed algorithm lies in its reasonably simple assumptions, calculations and hardware requirements. Furthermore, although the method successfully removes the bulk of the FPN in real IR data for different block lengths and compensates for the dead pixels of the video sequence, it exhibits ghosting artifacts as almost every

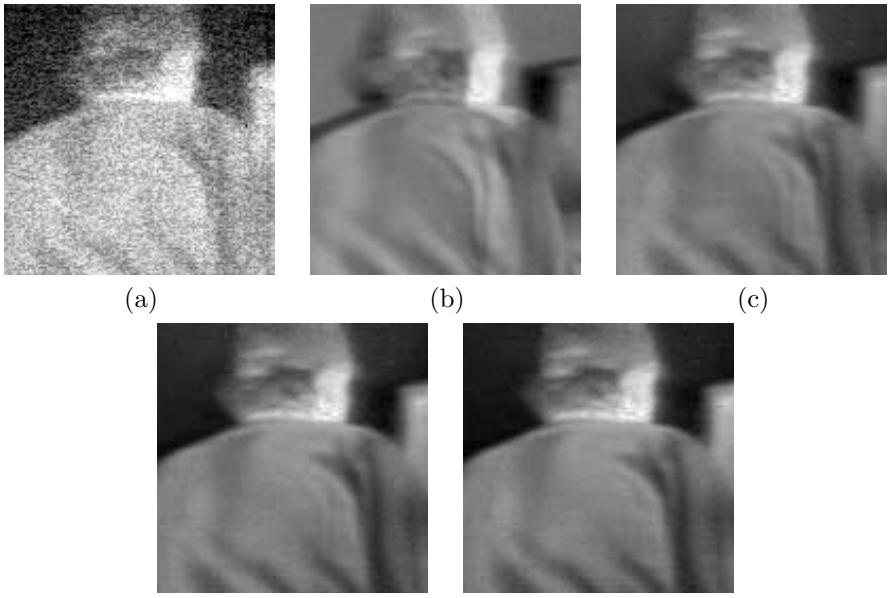

Figure 5. A sample IR image from the block of data of the FLIR Merlin camera corresponding to the $k = 200$th frame. (a) The raw image. The compensated versions of the raw image using: (b) the bias compensator algorithm with $K = 100$ frames, (c) the bias compensator algorithm with $K = 400$ frames, (d) the bias compensator algorithm with $K = 800$ frames, and (e) the bias compensator algorithm with $K = 1300$ frames

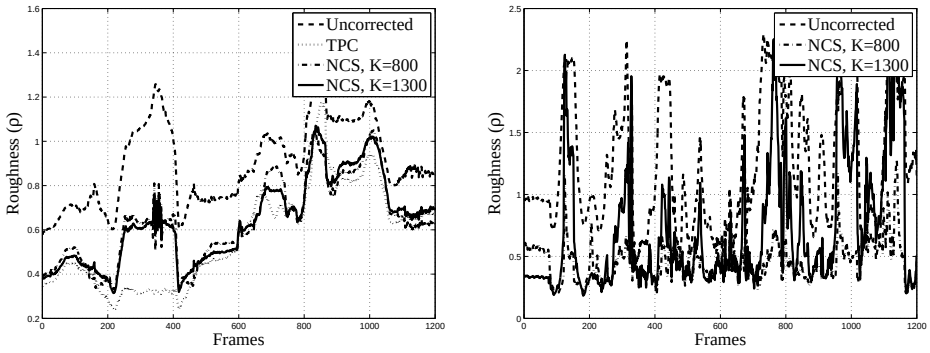

Figure 6. The calculated roughness coefficient ρ of the proposed algorithm for: (a) the AMBER camera data set; and (b) the FLIR Merlin camera data set.

scene-based NUC. An optimal value of the average MSE is given for 1300 frames per block for both cameras according to our judgment.

Notably the NC-based method resembles constants statistics when the LTI FIR is designed with only one coefficient. However for the NC method it is not necessary to have an integrated infrared irradiance with zero mean. More research need to be engage relate to motion depended and relate to simulate additive FPN with

two or tree flat images in the simulate reference sequence.

REFERENCES

1. M. J. Cantella, "Staring sensors systems." Printed Chapter Draft, April, 1992.
2. G. C. Holst., *CCD Arrays Cameras and Displays*, SPIE Press, JCD Publishing, 1996.
3. J. M. Lopez-Alonso, J. Alda, and E. Bernabeu, "Principal-component characterization of noise for infrared images," *Applied Optics* **41**, 2002.
4. D. A. Scribner, K. A. Sarkady, M. R. Kruer, J. T. Caulfield, J. D. Hunt, M. Colbert, and M. Descour, "Adaptive retina-like preprocessing for imaging detector arrays," in *Proc. IEEE Int. Conf. on Neural Networks (ICNN)*, pp. 1955–1960, 1993.
5. A. F. Milton, F. R. Barone, and M. R. Kruer, "Influence of nonuniformity on infrared focal plane array performance," *Optical Engineering* **24**, 1985.
6. P. M. Narendra and N. A. Foss, "Shutterless fixed pattern noise correction for infrared imaging arrays," in *Technical Issues in Focal Plane Development, Proc. SPIE*, W. S. Chan and E. Krikorian, eds., **282**, 1981.
7. J. G. Harris and Y.-M. Chiang, "An analog implementation of the constant average statistics constraint for sensor calibration," in *Advances in Neural Information Processing Systems*, M. C. Mozer, M. I. Jordan, and T. Petsche, eds., **9**, p. 699, The MIT Press, 1997.
8. U. Sakoglu, R. C. Hardie, M. M. Hayat, B. M. Ratliff, and J. S. Tyo, "An algebraic restoration method for estimating fixed pattern noise in infrared imagery from a video sequence.," *49th Annual Meeting of the SPIE: Applications of Digital Image Processing XXVII, SPIE Proc.* **5558**, 2004.
9. S. Haykin, *Adaptive Filter Theory*, Pretince-Hall, Inc., third ed., 1995.
10. J. Pezoa, M. M. Hayat, S. N. Torres, and M. S. Rahman, "Multi-model kalman filtering for adaptive nonuniformity correction in infrared sensors," *J. Optical Society of America A.* **23**, 2006.
11. B. M. Ratliff, M. M. Hayat, and J. S. Tyo, "Generalized algebraic scene-based nonuniformity correction algorithm.," *Journal of the Optical Society of America A.* **22**, February. 2005.
12. B. M. Ratliff, M. M. Hayat, and J. S. Tyo, "Radiometrically accurate scene-based nonuniformity correction for array sensors," *J. Optical Society of America A.* **20**, 2003.
13. S. N. Torres and M. M. Hayat, "Kalman filtering for adaptive nonuniformity correction in infrared focal plane arrays," *The Journal of Optical Society of America A.* **20**, 2003.